Fundamental Function of Linear Dipole Type DC Electric Field Sensor and Method for obtaining Reliable Electric Field Intensity

M.Tsutsui[1*]

[1] Retired from Kyoto Sangyo University in 2015

Corresponding author: Minoru Tsutsui (tsutsui@cc.kyoto-su.ac.jp)

†Professor Emeritus, Kyoto Sangyo University

Home address: 3-1-47, Nanryo-cho, Uji, Kyoto 661-0028, Japan

ORCID ID: https://orcid.org/0000-0003-4975-9010

Index Terms

0609 Antennas

0694 Instruments and techniques

6914 Electromagnetic noise and interference

Key Points:

- function of linear dipole type DC electric field sensor system was clarified, and analyzed its circuit parameters.
- A relation between output voltage of the sensor system and reliable electric field intensity was established
- Validity of the established relation was verified from the same field intensity measured by two sensors of different lengths

(The above elements should be on a title page)

Abstract

Linear dipole type DC electric field sensor was newly developed, and continuous observations by means of 3-D sensor system composed of three sensors installed orthogonally with each other have been conducting since 2017. However, their measured intensites have been remained uncertain, because they could not be calibrated from a reason that, at present, there dose not exist any facility for making uniform electric field in a wide area. So, in order to establish a method for obtaining reliable electric field intensity from output voltage of the sensor system, fundamental function of the sensor system has been examined. Since resistor *R* which is to be connected to input terminals of differential pre-amplifier is a key parmeter in the sensor system, it was needed to examin a characteristic curve of the output voltage as a fuction of *R*. For this purpose, simultaneout observations of natural electrioc fields were conducted by means of prural sensor systems installed in parallel. From obtained characteristic curve, an optimum value of *R* could be decided, and a formula showing a relation between reliable electric field intensity and output voltage of the sensor system was found. Validity of the formula has been verified by results of simultaneous observations of a lightning pulse by means of two vertical sensor systems whose element lengths were different. Their results have shown same electric field intensity. As the result, the linear dipole type DC electric field sensor system with the formula has been perfectly established as a practically useful sensor system.

Plain Language Summary

Natural electric fields whose property had so far not been clear were observationally clarified by a newly developed DC electric field sensor system in 2020. However, measured electric field intensities have been remained uncertain, because they could not be calibrated from a reason that, at present, there dose not exist any facility for making uniform electric field in a wade area. This paper describes a procedure to find a mthod for obtaining reliable intensity of electric field from output voltage of the sensor system, in which fundamental function of the sensor system has been clarified through analysis of circuit parameters of the system, combining with test observations of natural electric fields by means of prural sensor systems installed in parallel. From these analysis, a formula showing a relation between reliable electric field intensity and output voltage of the sensor system has been found. Validity of the formula was verified by simultaneous observations by means of two vertical sensor systems in which lengths of sensing elements were different. Their measured results have shown the same electric field intensity. Therefore, the linear dipole type DC electric field sensor system with the formula has been perfectly established as a practically useful sensor sysrtem.

1 Introduction

Linear dipole type DC electric field sensor was developed (Tsutsui and Kaji, 2020). Since the laboratory experiment of its small proto-type sensor had clearly indicated an angular dependence of electric field components against the direction of a uniform electric filed, practical observations of natural electric field had been conducted by means of a 3-D sensor system composed of three linear dipole elements set orthogonally with each other, and showed that the detected electric fields were ionosphere Sq electric fields. However, the measured electric field intensities have been remained uncertain, because they could not be calibrated due to hardness of making a uniform electric field in a wide area. Therefore, I began to find a method for obtaining reliable electric field intensities from output voltage of the sensor system. For this purpose, I have been examining fundamental function of the sensor system.

2 Important points in detection of DC electric field

As shown in the original paper (Tsutsui and Kaji, 2020), the linear dipole type DC electric field sensor system is composed of two parts. One is a structure of linear dipole sensing elements including feeding cable, and another is a transforming function of a whole sensor system from external electric field to an output voltage of differential pre-amplifier. For the first part, a new structure of the sensing part including feeding cable had been already developed before 2017, and it had been used for observations since 2017. So, I would like to open here its structure especially for DC electric field detections. On the other hand, the investigation of the transforming function of this sensor system is a main subject of this paper, because the characteristics of differential pre-amplifier connected by input resistors affects accuracy of measured electric field intensity.

2.1 A new structure of sensor elements for keeping electric balances

Figure 1 shows a basic form of electric circuit of linear dipole type DC electric field sensor (Tsutsui and Kaji, 2020). The dipole sensor is drawn symmetrically as a T-shaped structure. In VHF radio communications, symmetrically structured dipole antennas (Uda and Mushiake, 1954) are important for transmitting pure sinusoidal forms of electromagnetic waves in space. Even in measurements of DC electric field, electrical balance between the dipole elements is important. For sensitive detections of DC electric field, a pair of co-axial cables is essential for feeding DC potentials from twe sensing elements to a differential pre-amplifier in order to guard permeations of unexpected potentials from other parts besides the dipole elements. In this case, the co-axial cables have to be fixed rigidly during observations, otherwise the electric balance was not warranted, because spacings between the outer mesh (at the ground potential) of the co-axial cables and two sensing elements in the T-shaped feeding situation shown in Fig. 1 would be fluctuating by their swaying due to wind, and detected DC potential difference had been always fluctuating even if static DC electric field was forming in a space around the dipole elements. As the result, effects of the ground potential to the two dipole elements are fluctuating all times.

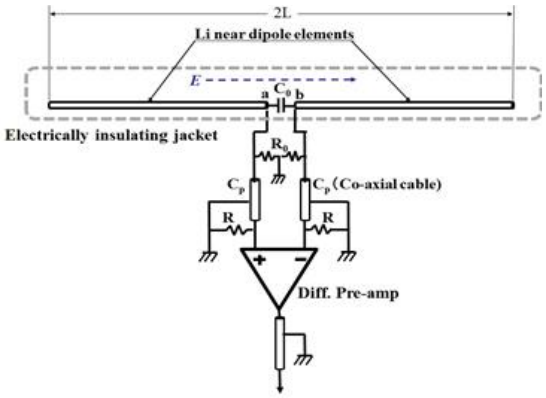

Fig. 1 Basic electric circuit of linear dipole type DC electric field sensor which has been used for observations since 2017, and observed results are described in the paper (Tsutsui and Kaji, 2020). C_0 is a capacitance to shunt AC noise picked up on the dipole elements. R_0 was used for flowing small current between the two linear dipole elements and for obtaining DC potential difference between them. Resistor R was used for a return path of bias current at gate of FETs in front-end circuit of a differential pre-amplifier in order not to charge-up stray capacitance at the gate of FET. C_p is capacitance formed between inner line and outer mesh of co-axial feeding cables.

For solving the problem, I came up with a distinguished structure for the linear dipole type DC electric field sensor and its feeding method, which is shown in Fig. 2. The electric circuit in Fig. 2 is quite the same as that in Fig. 1, but their structures are quite different. I call it “I-shaped linear dipole sensor”. In Fig.2, a pair of feeding co-axial cables are threaded insides of two cylindrical sensing elements. By this structure, spacings between the two cylindrical elements and the outer mesh (at the ground potential) of the pair co-axial cables are always fixed rigidly. Therefore, the effects of the ground potentials to the two cylindrical dipole elements are always balanced and fixed at all times.

I conducted comparison measurements of natural electric fields between by the T-shaped dipole sensor (Fig. 1) and by the I-shaped one (Fig. 2), and confirmed that DC potentials measured by the T-shaped sensor were rather fluctuating than those of I-shaped one. Then I am confident that the I-shaped sensor is very sensitive in detections of DC electric fields than the T-shaped one, and I have been using the I-shaped sensors in observations since 2017, and their data were used in the original paper (Tsutsui and Kaji, 2020).

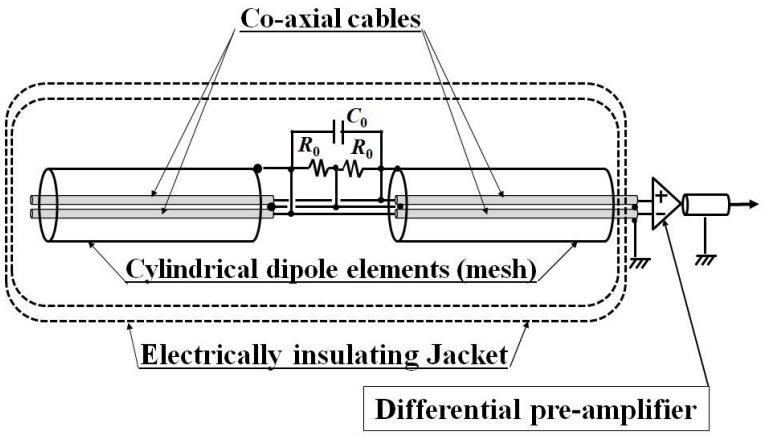

Fig. 2 Improved (I-shaped) structure of linear dipole type DC electric field sensor. Its electric circuit is quite same as that of T-shaped sensor shown in Fig, 1. Since two co-axial cables are threaded inside of two cylindrical dipole sensing elements, spacings between the two cylindrical elements and the outer conductive mesh (at the ground potential) of the pair of co-axial cables are same and fixed rigidly. Therefore, effects of the ground potential to the cylindrical elements are always balanced. I-shaped sensors have been used in observations since 2017. At present, two R_0 connected between the two sensing elements and the ground seen in the figure are removed from all sensors from the reason obtained in the present study.

2.2 Effect of input resistor of differential pre-amplifier

The principle of measurement of electric field intensity E in a space is to measure a potential difference (V_a-V_b) between points **a** and **b** (the distance L) of two floating conductive items set in the space, and to obtain E=(V_a-V_b)/L. Thus, a differential pre-amplifier with high input impedance is the best electric device to measure it. However, for measurements of DC electric field, some C-R circuit have to be connected to input (+,-) terminals of differential pre-amplifier for reducing AC noise on the floating conductive items. So, I tentatively connected C_0 and $2R_0$, where C_0= 10 μF and R_0= 470 kΩ, between the dipole elements as shown in Fig. 1. On the other hand, Data sheet of a differential pre-amplifier INA 110 (INA 110 Burr-Broun product) which I have been using describes that it is recommended to connect resistors R (1 MΩ) between input terminal of the differential pre-amplifier and the common (GND) when it is used for measuring potentials of floating sources, because the resistor R is used for a return path of bias current from the gate of FET, in order to prevent charging-up of stray capacitance at the gate of FET. So, I also connected the resistors R (R= 1MΩ) as shown in Fig. 1, and had been continuing observations since 2017.

Without any intention before the present study, I checked the output voltage of the differential pre-amplifier by changing the value of R connected to its input terminal, and found that the output voltage of INA 110 easily increased when the value of resistor R was increased from 1 MΩ, and that this sensor system showed "R-dependent characteristics". So, I perceived that it should be clarified the fundamental function of the whole sensor system, and the sensor system should be made to be "R-independent" one.

3 Analysis of circuit parameters of linear dipole type DC electric field sensor system

3.1 Equivalent electric circuit of the sensor system

A main purpose in the present analysis is to clarify "*R*-dependent" output voltages of differential pre-amplifier INA 110. By applying the Kirchhoff's law to the electric circuit in Fig. 1, its equivalent electric circuit was obtained as in Fig. 3(a). In Fig. 3(a), a physical image of the linear sensing elements is shown. By external electric field, charges within the conductive linear dipole elements would be separated to their both ends. Due to the charge separations, another electric field of $-E$ would be formed within the linear elements in the direction inverse to that of the external electric field. Thus, the linear elements can be regarded as a kind of storage battery, and voltage V_E would emerge between both ends of the element given by $V_E = E \times L$, where L is the length of the single linear element. Thus. the voltage V_E of the battery is always induced by the external electric field E, and a current ***i*** from the battery is also flowing out to the load (resistor R). When the current is flowing to the load, an internal impedance emerges in the battery as a current dependent form of $Z_g(i)$.

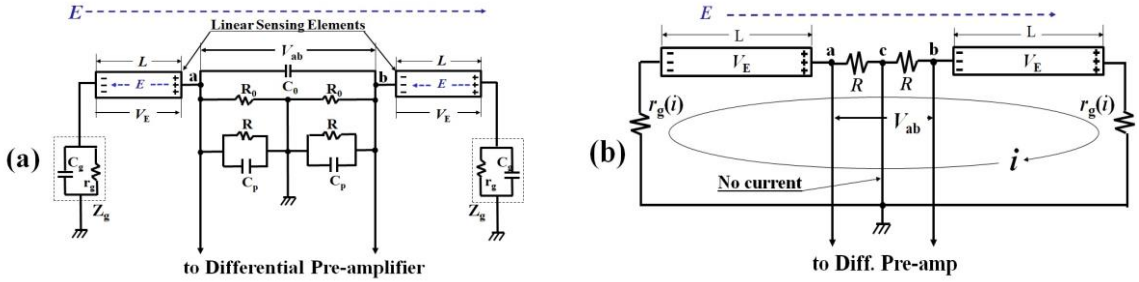

Fig. 3 **(a)** shows an equivalent electric circuits of linear dipole type DC electric field sensor system derived from the circuit shown in Fig. 1 by applying Kirchhoff's law. By external electric field, charges + and – within the sensing elements are separated to their both ends. Due to the charge separations, another electric field (-*E*) is formed within each sensing element in the direction inverse to that of the external electric field. As the result, a voltage V_E emerges between both ends of the linear element as $V_E = E \times L$, where L is the length of a sensing element. Therefore, the circuit can be simplified as that in (b)**.** **(b)** shows further equivalent electric circuit simplified from (a). Because R_0 and R had been connected in parallel, R_0 can be removed for simplifying the analysis of "*R*-dependent" output voltage of differential pre-amplifier. Capacitances C_0 and C_p can be also neglected hereafter because of the analysis of very low frequency (near DC) potentials. V_E is always induced by the external electric field and is flowing small current ***i*** to a load R. At the same time, current dependent internal resistance $\boldsymbol{r}_g(\boldsymbol{i})$ emerges.

For making the analysis simplify, the resistor R_o can be removed because it had been parallelly connected with R. Furthermore, the capacitances C_0 and C_p can be neglected because of the analysis of DC potentials, and $Z_g(i)$ became $r_g(i)$. As the result, its circuit becomes as that in **(b)**. In **(b)**, only one current ***i*** is flowing in the total system through $2R$ between **a** and **b**. In this case, no current is flowing along the line between point **c** and the ground, because the same currents from the induced voltages V_E of two linear elements are flowing in the line inversely with each other. As the result, the resistor R plays two roles. One is measurements of the current flown between the two sensing elements, and another is the return path of bias current from the gate of FET in the front-end circuit of INA110 as decribed in its data sheet. The analysis of circuit parameters in (b) is proceeded hereafter.

A main formula for the circuit shown in Fig. 3(b) is given as $2V_E = i\,\{2R+2r_g(i)\}$, and then

$$V_E = i\,\{R + r_g(i)\}. \tag{1}$$

Thus the current i can be given as

$$i = \frac{V_E}{\{R + r_g(i)\}}\,. \tag{2}$$

Since the potential at point **c** is fixed to the ground (GND), potential $V_a(R)$ at point **a** against the GND is given as

$$V_a\,(R) = Ri = \frac{RV_E}{\{R + r_g(i)\}} = \frac{V_E}{\{1 + r_g(i)/R\}}. \tag{3}$$

Similarly, the potential $V_b(R)$ at point **b** against the GND also becomes as

$$V_b(R) = -\frac{V_E}{\{1 + r_g(i)/R\}}. \quad (4)$$

As the result, the potential difference $V_{ab}(R)$ between point **a** and **b**, which is just the output voltage of differential pre-amplifier of the sensor system, becomes as

$$V_{ab}(R) = V_a - V_b = \frac{2V_E}{\{1 + r_g(i)/R\}} m\,, \quad (5)$$

where m is the amplification factor of the differential pre-amplifier. This formula suggests that, even if the voltage V_E is constant, the voltage $V_{ab}(R)$ varies when the value of resistor R was changed. Therefore, forms of R-dependent $V_{ab}(R)$ at a moment have to be clarified, and the value of R should be fixed for obtaining a relation between V_E and $V_{ab}(R)$.

Since V_E induced by natural electric field E(t) is changing from time to time, it is needed to examine $V_{ab}(R)$ in a time-independent situation. A way to find "time-indepent formula of $V_{ab}(R)$" is to delete V_E by taking a ratio of $V_{ab}(R_1)$ to $V_{ab}(R_2)$ for different values of R_1 and R_2 as

$$\frac{V_{ab}(R_1)}{V_{ab}(R_2)} = \frac{2\dfrac{V_E}{\{1 + r_g(i_1)/R_1\}} m}{2\dfrac{V_E}{\{1 + r_g(i_2)/R_2\}} m} = \frac{\{1 + r_g(i_2)/R_2\}}{\{1 + r_g(i_1)/R_1\}}. \quad (6)$$

This formula expresses a time-independent relation between output voltages $V_{ab}(R)$ and internal resistances $r_g(i)$ of the sensor system shown in Fig. 3(b) for different values R_1 and R_2.

A method for obtaining $V_{ab}(R_1)$ and $V_{ab}(R_2)$, , , for different values of R_1, R_2, , , , in the time-independent situation is to conduct observations of natural electric fields by means of plural sensor systems whose structural specifications are quite the same, but resistors R_1, R_2, , , , having different values are connected to differential pre-amplifier in each sensor system.

3.2 Practical method for obtaining time-independent form of $V_{ab}(R)$

In order to obtain time-independent $V_{ab}(R)$ as a function R, test observations by means of three dipole sensors were conducted. Figure 4 is a picture showing three dipole sensors, in which I-shaped sensor (Fig. 2) were set in north-south direction having separations of every 60 cm from the original one for avoiding interference among them. Structural specifications of these three sensors were quite the same, but different values of resistors R_1, R_2 and R3 were connected to input terminals of differential pre-amplifier in each sensor system. Since, from these systems, values of $V_{ab}(R_1)$, $V_{ab}(R_2)$ and $V_{ab}(R_3)$ were measured simultaneously, a rough form of $V_{ab}(R)$ as a function of R can be obtained, in which the same value of V_E (t) would be always induced on the three dipole elements at an instant though.

Fig. 4 Picture of three linear dipole elements of DC electric field sensors (I-shaped) installed at a hight of 4 m, and parallelly along north-south direction with separations of every 60 cm. Their structural specifications are quite same although different values of resistors R_1, R_2 and R_3 were connected to input terminals of differential pre-amplifier in each sensor system.

3.3 Simultaneously measured $V_{ab}(R)$ and current $i_{ab}(R)$

Fig. 5 shows plots of $V_{ab}(R)$ simultaneously measured by three sensor systems shown in Fig. 4. Fig. 5(a) shows a series of three plots of $V_{ab}(R)$ values when resistors of R_1=0.5MΩ, R_2=1MΩ and R_3=2 MΩ were connected to each differential pre-amplifier of three sensor systems whose amplification factor m were 500. They were observed during the period from Nov. 18 to 27 in 2020. (b) shows those when resistors of R_2=1MΩ, R_3=2MΩ and R_4=4MΩ were connected to each differential pre-amplifier whose amplification factors were m=500 except for that connected by R_4=4 MΩ was m=200. They were observed during the period from Nov. 29 to Dec.11 in 2020. In (a) and (b), three 24-hour traces of time-dependent $V_{ab}(R)$ are exemplified, and values of selected peaks measured at the same time in the three traces were read and plotted as indicated by arrows. In (a), $V_{ab}(R)$ trends in the range between resistors R_1=0.5MΩ and R_2=1MΩ show steep increasings, and those in the range between resistors R_2=1MΩ and R_3=2MΩ become rather gentle gradient. In (b), trends in the range of R higher than R_3=2MΩ show slowly increasing gradients and tend to constant values. Those plots in (a) and (b) indicate that all over the $V_{ab}(R)$ forms show only increasing trends as a function of R. Among these data, red-colored blanches on Nov. 19 and Dec. 3 in 2020, which seem to be connecting smoothly from R_1= 0.5 MΩ to R_4=4 MΩ, were selected out for further analysis.

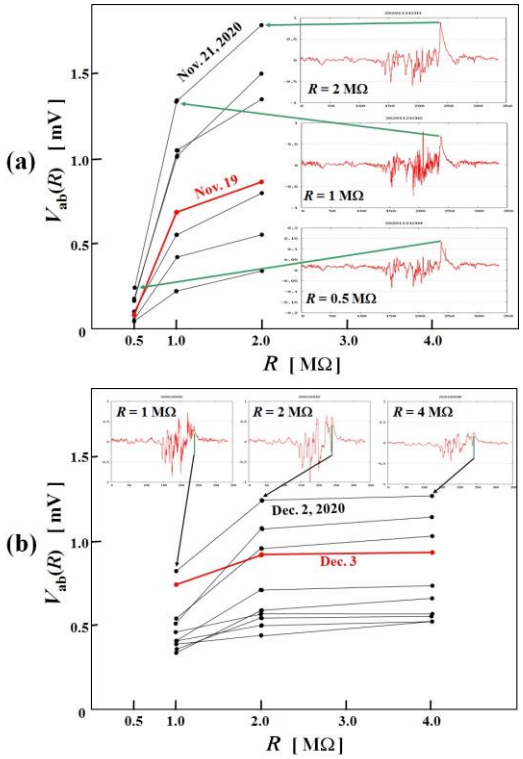

Fig. 5 Plots of $V_{ab}(R)$ simultaneously measured by three sensor systems, in which different values of resistors R were connected to each differential pre-amplifier. **(a)** shows series of three plots of values of $V_{ab}(R)$ measured when R_1=0.5MΩ, R_2=1MΩ and R_3=2MΩ were connected. They were observed during the period from Nov.18 to 27 in 2020. **(b)** shows those measured when R_2=1MΩ, R_3=2MΩ and R_4=4MΩ were connected, and were observed during the period from Nov. 29 to Dec. 11, 2020. In both **(a)** and **(b)**, three 24-hour traces of $V_{ab}(R)$ measured by three sensors systems are exemplified, and peak values at the same time are plotted as indicated by arrows. Amplification factors of differential pre-amplifiers were m=500 except for that connected by R_4=4MΩ was m=200. In units on the vertical axes, m is taken into account. Red-colored branches were selected out for further analysis below.

For obtaining current-dependent internal resistance $r_g(i)$ in Eq.(6), plots of R-dependent current $i_{ab}(R)$ were needed to be obtained. Values $i_{ab}(R)$ flowing through $2R$ were obtained by the relation of

$$i_{ab}(\mathrm{R}) = \frac{V_{ab}(R)}{2Rm}, \qquad (7)$$

where m is the amplification factors of each pre-amplifier. Resultant plots of $i_{ab}(\mathrm{R})$ are shown in Fig. 6. They show steeply increasing trends in the range between R_1= 0.5 MΩ and R_2 = 1 MΩ, peaks at R_2 = 1MΩ, and then gradual decreasing trends in the range higher than R_2 = 1 MΩ.

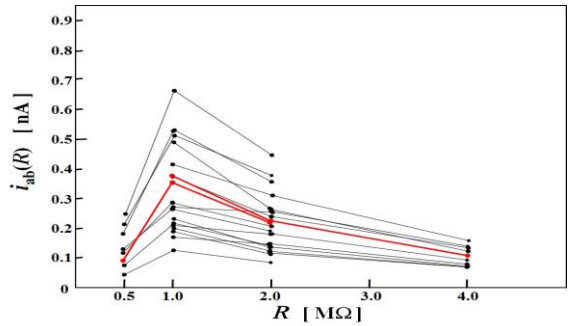

Fig. 6 *R*-dependent currents $i_{ab}(R)$ obtained from Eq. (7). Variations of $i_{ab}(R)$ show steep increases in the range between R_1= 0.5MΩ and R_2=1MΩ, peaks at $R2$= 1MΩ, and then gradual decrease in the range between R_2=1MΩ and R_4=4 MΩ. Red-colored branches are used for further analysis.

One pair of *R*-dependent forms of $V_{ab}(R)$ and $i_{ab}(R)$ selected out from Fig. 5 and 6 are plotted in Fig. 7. In the range between R=0.5 MΩ and R=1 MΩ, they show both steep increasing trends, and show opposite trends with each other in the range R > 1 MΩ.

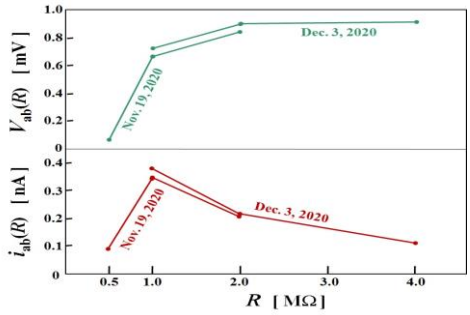

Fig. 7 $V_{ab}(\mathrm{R})$ and $i(R)$ forms as functions of R selected from Fig. 5 and 6. In the range between R_1= 0.5MΩ and R_2=1MΩ, both forms show steep increasing trends whereas those in the range of R higher than R_2=1 MΩ show opposite (increasing and decreasing) trends, respectively. Physical meaning of their increasing trends in the range between R_1= 0.5MΩ and R_2=1MΩ is explained below.

3.4 Internal resistance $r_g(i)$

Eq. (6) shows a ratio of $V_{ab}(R_1)$ to $V_{ab}(R_2)$ for different resistor values R_1 and R_2, and also related to $r_g(i_1)$ and $r_g(i_2)$. From this formula, an internal resistance value $r_g(i_1)$ can be obtained when resistor values of R_2 is very close to R_1, as given by $R_2 = R_1+\Delta R$, where ΔR is extremely small. In this case, value of $r_g(i_2)$ can be regarded as that of $r_g(i_2)$. Then $r_g(i_1)$ can be derived approximately from Eq, (6) by putting $r_g(i_2) \approx r_g(i_1)$, as

$$r_g(i_1) \approx \frac{V_{ab}(R_1+\Delta R) - V_{ab}(R_1)}{\frac{V_{ab}(R_1)}{R_1} - \frac{V_{ab}(R_1+\Delta R)}{R_1+\Delta R}} \approx -\frac{\Delta V_{ab}(R_1)}{\Delta i(R_1)}. \qquad (8)$$

This result means that the internal resistance $r_g(i)$ emerges in each storage battery is given by a ratio of a small difference of detected voltages $\Delta V_{ab}(R_1)$ to its related small difference of current $\Delta i(R_1)$ in a small range ΔR between R_1 and $R_1+\Delta R$. An important point in Eq. (8) is (-) sign, which means that there exists a case that $r_g(i)$

has negative values. In the present analysis, the resistance value of $r_g(i)$ should be positive, and its negative value is inconceivable. Therefore, if the negative value of $r_g(i)$ emerged, other physical mechanism has to be reconsidered, which is discussed later. The condition showing positive $r_g(i)$ is only the case when $V_{ab}(R)$ and $i(R)$ as a function R indicate opposite (increasing versus decreasing, and vice versa) trends with each other.

Since measured data $V_{ab}(R)$ and $i(R)$ were discrete values for discrete values of R_1, R_2, R_3 and R_4, values of $r_g(i)$ become constant in the ranges between two values of R. So, descriptions of $r_g(i)$ in Eq. (8) can be modified as,

$$r_g(R_1 \sim R_2) = -\frac{V_{ab}(R_2) - V_{ab}(R_1)}{i_{ab}(R_2) - i_{ab}(R_1)}, \qquad (9)$$

and the value of $r_g(R_3)$ at R_3= 2 MΩ can be obtained as the form of

$$r_g(R_3) = \frac{r_g(R_2 \sim R_3) + r_g(R_3 \sim R_4)}{2}. \qquad (10)$$

As the results, constant values of $r_g(R_n \sim R_{n+1})$ and $r_g(R_n)$ are plotted in Fig.8 although it is expected that the practical $r_g(R)$ would change continuously as shown by a continuous broken line in the figure for continuously changing value of R. Their values are $r_g(1\sim2)$ = 1.21 MΩ and 1.19 MΩ, $r_g(2)$ = 0.66 MΩ and $r_g(2\sim4)$ = 0.13 MΩ. On the other hand, the negative value $r_g(0.5\sim1)$ = -2.34 MΩ was obtained because both $V_{ab}(R)$ and $i_{ab}(R)$ in the range between R_1=0.5 and R_2=1MΩ show same increasing trends as a function of R as seen in Fig. 7. The reason of the same increasing trends is deliberated below.

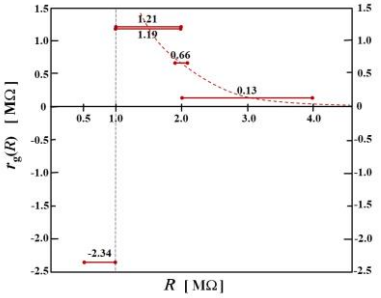

Fig. 8 Internal resistance values $r_g(R)$ obtained by Eq. (9) and (10). Negative value $r_g(0.5\sim1)$ = -2.34 MΩ is shown only in the range 0.5< R < 1.0 MΩ. Positive values of $r_g(R)$ shown in the ranges R > 1 MΩ were applied to the present analysis.

[About negative value of $r_g(0.5\sim1)$**]**

Before the present study, an unexpected fact had been found. As described at the end part in **2.2**, I found a strange result during the check of the sensor system (the first case) that the output voltage of INA 110 easily increased when the value of R in Fig. 1 was increased from 1 MΩ. Another fact was found in the test observation at the beginning of the present study (the second case), in which after removal of R_0 and replacing R by R_1= 0.5 MΩ, I tried to increase the value of R_1 a little bit form 0.5 MΩ, then similar increasing occurred in $V_{ab}(R)$ and $i_{ab}(R)$. At that time, I noticed that the phenomena in both cases would be occurred by the same cause, that is the connections of resistors having very low values. In the first case, the total value of resistance was 0.32MΩ because of parallel connections of R_0 = 0.47MΩ and R = 1MΩ, and, in the second case, just a low value resistance of 0.5 MΩ was connected. It has been considered that the connections of such very low resistances would derange the originally designated bias-voltage for the FET in the front-end circuit of pre-amplifier (INA 110).

From text books on amplification mechanism of FET circuit, the above phenomena can be understood. In a situation that the best bias voltage at the gate of FET in the front-end circuit of an amplifier is originally designated, if a resistor R_1=0.5MΩ was connected to the gate of FET against the ground, its resultant resistance value in the circuit would become abnormally lower than the originally designated value. Thus, the bias voltage would also down from the originally designated one. Then, if the resistance value of R_1 was increased a little bit from 0.5MΩ in the abnormal situation, the bias voltage at the gate would be increased and then the collector

current of the FET circuit would increase. So, the output voltage of the INA 110 $V_{ab}(R)$ would be increased simultaneously, and $i_{ab}(R)$ show the same increasing trends as a functions of R.

As the conclusion, it is considered that this abnormal situation was caused due to deranging the normal biasing-circuit, by connecting very low resistance to the gate of the FET. This thinking would be valid, because the abnormal phenomena did not occur when R_2=1MΩ only was connected to the input terminal of INA 110 for return path of bias current from the gate of FET as described in the INA 110 Data Sheet.

I have recognized, from this consideration, that the electric field intensities which were measured in the observations in 2017 (Tsutsui and Kaji, 2020) were incorrect, because the observations had been continued in the situation of parallel connections (R_0//R =0.32 MΩ) as seen in Fig.1.

3. 5 Relation between $V_{ab}(R)$ and $V_E(R)$

Since, $V_{ab}(R)$ and $i_{ab}(R)$ show opposite trends in the range of R lager than 1MΩ in Fig. 7, positive values of $r_g(R)$ were obtained as shown in Fig. 8. So, they could be applied to the present analysis. Since the form of V_E in Eq. (1) can be rewritten as

$$V_E(R) = i_{ab}(R)\{R + r_g(R)\}. \qquad (11)$$

From observations, $V_{ab}(R)$ and $i_{ab}(R)$ at R were obtained and their related $r_g(R)$ was derived as in Fig. 8. Then, by putting these values into Eq. (11), induced voltages $V_E(R)$ can be obtained. So, a relations between $V_{ab}(R)$ and $V_E(R)$ is shown in Fig. 9. $V_{ab}(R)$ and $V_E(R)$ in this figure are changing with the value of R, which means R-dependent ones. For example, they show $V_{ab}(R_3)$ = 0.92 mV and $V_E(R_3)$ = 0.61 mV at R_3=2MΩ, which means $V_E(R_3) = 0.66 \times V_{ab}(R_3)$. Furthermore, they show $V_{ab}(R_4)$ = 0.94 mV and $V_E(R_4)$ = 0.48 mV at R_4 = 4MΩ, which means $V_E(R_4) = 0.51 \times V_{ab}(R_4)$, and it is very close to $V_{ab}(R_4)/2$ with an error of 2%. It is regrettable that more sensor systems having higher values of R (for example, R_5= 5MΩ, R_6= , R_7= , , ,) had not been added in the test observation (Fig. 4) for confirming a relation of $V_E(R_5) = V_{ab}(R_5)/2$ from trends indicated by broken arrows in the figure.

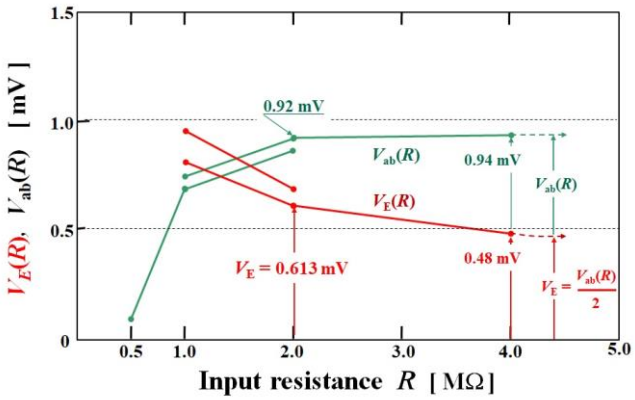

Fig. 9 Trends of measured voltage $V_{ab}(R)$ and derived $V_E(R)$ when the value of the resistor R connected to the input terminal of differential pre-amplifier (INA 110) was regarded to have been changed from 0.5 MΩ to 4.0 MΩ. Since $V_E(R) = 1.02\ \frac{V_{ab}(R)}{2}$ was obtained at R= 4MΩ, it is expected that V_E(R) would tend to $\frac{V_{ab}(R)}{2}$ for higher value of resistor R (>>5 MΩ) as indicated by broken arrows.

It is fully expected to be $V_E(R) = V_{ab}(R)/2$ from the trend of $V_{ab}(R)$ for higher value of R. Because $V_{ab}(R)$ in Fig. 5(b) would tend to almost constant (horizontal) for higher value of R >>4. In this case, $V_{ab}(R)$ became "R-independency", and since the numerator of Eq. (9) would tend to zero, $r_g(R)$ would become negligibly small ($r_g(R)$ -->0). Thus, $V_E(R)$ would also become to R-independent value as

$$V_E(R) = \frac{V_{ab}(R)}{2Rm} \times (R + 0) = \frac{V_{ab}(R)}{2m}, \qquad (12)$$

where m is the amplification factor of INA 110, and it means "R-independent" V_E.

As the conclusion, the present analysis has shown that "*R*-independent voltage V_E" can be obtained whenever enough higher value of resistor R (>5 MΩ) was connected to the input terminal of pre-amplifier. Therefore, by deciding an "optimum value of R_{opt} (= 10 MΩ was deided in this paper), the voltage $V_E(R_{opt})$ is given by the value of just a half of the measured voltage ($\frac{V_{ab}(R_{opt})}{2m}$). As the conclusion, reliable electric field intensity E can be obtained by a relating formula

$$E = \frac{V_{ab}(R_{opt})}{2Lm}, \qquad (13)$$

where L is the length of a sensing element of the dipole sensor and m is the amplification factor of differential pre-amplifier.

4 Validity of developed method for obtaining reliable electric field intensity

In the present study, I have established a method for obtaining reliable electric field intensity along the linear dipole elements as shown in Eq. (13).

A way to prove the validity of the form $E = \frac{V_{ab}(R_{opt})}{2Lm}$ is to measure natural electric fields simultaneously by means of multiple linear dipole sensor systems whose element lengths are different, and to show that measured results from their sensor systems could provide the same electric field intensity. In order to confirm it, I installed two electric field sensors having elements of 2.5 m and 1m in length, respectively. Figure 10 shows a picture of two vertical sensors (E_{v_5m} and E_{v_2m}) whose total length 2L are 5 m and 2 m, respectively, and spacing between them is 2.6 m above roofs of buildings at a corner of residential area. R_{opt} =10 MΩ was connected to the input terminal of INA 110 in each sensor system, and its amplification factors of both differential pre-amplifiers were m=10.

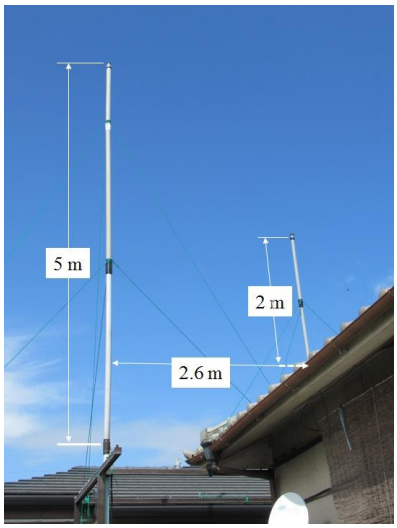

Fig. 10 Two vertical linear dipole type DC electric field sensors (E_{v_5m} and E_{v_2m}) whose sensor elements are I-shaped structure of 5 and 2m in total length 2*L*, respectively. They were installed having a spacing of 2.6m just above roofs of buildings at a corner of residential area.

Observed 24-hour traces of these sensor systems are shown in Fig. 11, in which vertical axes on the left-hand side indicate measured voltages of V_{ab}(10MΩ)/m, and those on the right-hand side indicate electric field intensity derived from $E = \frac{V_{ab}(10M\Omega)}{2Lm}$. Both traces show similar fluctuating forms except for the part indicated by **a**. The source of a large swinging form seen on the trace of E_{v_5m} was a lightning pulse occurred at far distance from those sensors although it is barely seen on that of E_{v_2m}. These results suggest that longer dipole sensor is sensitive than that of shorter one.

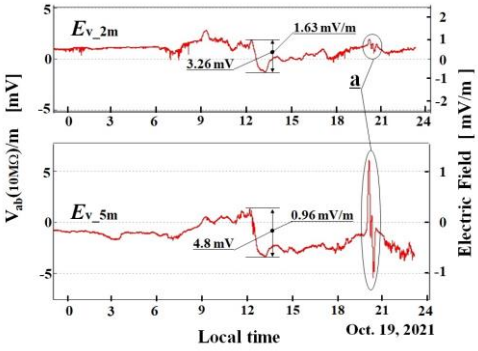

Fig.11 24-hour traces of $V_{ab}(10M\Omega)/m$ detected by two vertical linear dipole type DC electric field sensors E_{v_2m} and E_{v_5m}, respectively. Axes on the left-hand side indicate measured voltages $V_{ab}(10M\Omega)/m$ in each sensor system, and those on the right-hand side indicate electric field intensities. A large swinging form of a lightning pulse occurred at far distance is clearly seen in the part of **a** on the trace of E_{v_5m} although it is barely seen on that of E_{v_2m}.

Furthermore, their time-expanded traces seen in the part **a** in Fig. 11 are shown in Fig. 12, in which both traces have shown the similar forms of electric field intensity although those in Fig. 11 seems to be quite different. Both peaks indicate almost the same value of about 1mV/m as pointed by horizontal broken arrows.

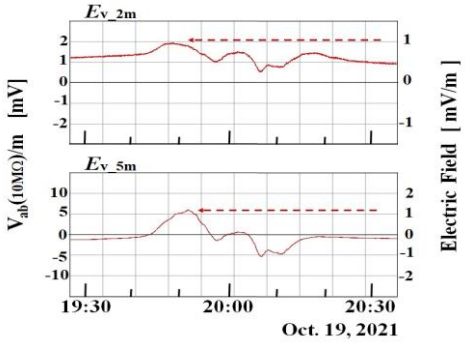

Fig. 12 Time-expanded traces in the part **a** in Fig. 11. Since both traces show similar fluctuating forms, their electric fields would have been coming from one lightning pulse. Peak values of the lightning pulse detected by E_{V_2m} and E_{V_5m} are shown as the same value of 1mV/m as indicated by horizontal broken arrows.

The result has shown that the method developed in the present study is the best way for obtaining reliable electric field intensity and can be fully applied to all linear dipole type DC electric field sensors whose element lengths are different.

5 Conclusions

Values of electric field intensity measured by the linear dipole type DC electric field sensor developed in 2020 (Tsutsui and Kaji, 2020) have been remained uncertain, because they could not be calibrated due to non-existence of facility for forming uniform electric field in a wide space. Then I have been developing a method for obtaining reliable electric field intensity from output voltage of the sensor system. Through the detailed analysis of an equivalent electric circuit of the sensor system, R-dependent output voltage $V_{ab}(R)$ of the sensor system has been crarified, where R is value of resistor connected to input (+, -) terminals of the differential pre-amplifier. Since, for fully higher value of R (>> 5 MΩ), the sensor system became R-independency, an optimum

value of R was decided as R_{opt} = 10 MΩ in this paper. Then electric field intensity E around sensing elements could be obtained by the relation of $E = \frac{V_{ab}(R_{opt})}{2Lm}$, where L is the length of single sensing element of the dipole sensor and m is the amplification factor of the differential pre-amplifier. Validity of the established formula has been verified from observations by means of two vertical linear dipole sensors whose element lengths were L= 2.5m and 1m, respectively, and have shown that both sensors provided the same electric field intensity.

By the present study, a set of the improved linear dipole sensor system with a formura showing a relation between output voltage of the sensor system and electric field intensity has been perfectly established as a linear dipole type DC electric field sensor system. So, it is expected that net-work observations by this sensor systems would provide new findings about electro-magnetic phenomena around the globe and outer space.

Acknowledgments

I thank Hiroshi Oya, and Tohru Araki for their valuable discussions and comments on the present study.

References

Tsutsui, M and R. Kaji: "A New DC Electric Field Sensor and Direct Measurements of Ionosphere Sq Electric Fields", IEEJ Trans 2020; **15**: 1271-1280. Published online in Wiley Online Library (wileyonlinelibrary.com). DOI:10.1002/tee.23193.

Uda, S. and Y. Mushiake, "Yagi-Uda antenna" Maruzen (1954).

INA 110 Burr-Brown Products from Texas Instruments:
Fast-Settling FET-Input INSTRUMENTATION AMPLIFIER
https://www.ti.com/lit/ds/symlink/ina110.pdf?ts=1642038973527&ref_url=https%253A%252F%252Fwww.google.com%252F